第 34 卷第 2 期
2018 年 2 月

无 机 化 学 学 报
CHINESE JOURNAL OF INORGANIC CHEMISTRY

Vol.34 No.2
277-282

Zintl 相化合物 α-$BaZn_2P_2$ 的合成、结构和性能

白明成[1,2] 潘明艳[2] 汪 琳*[,1] 齐红基[2] 王 虎[2]

([1]上海大学材料科学与工程学院,上海 200444)

([2]中国科学院上海光学精密机械研究所,强激光材料重点实验室,上海 201800)

摘要:通过 Sn 助熔剂法在高温下合成一种 Zintl 相化合物 α-$BaZn_2P_2$,通过 X 射线单晶衍射确定其晶体结构与 α-$BaCu_2S_2$ 同构,属于 *Pnma* 空间群。α-$BaZn_2P_2$ 的晶格参数为:a=0.976 78(5) nm,b=0.413 34(2) nm,c=1.060 55(5) nm。与高温相 β-$BaZn_2P_2$ 的层状结构不同,低温相 α-$BaZn_2P_2$ 具有三维网格结构。其中 ZnP_4 四面体通过共边和共顶 2 种方式连接形成阴离子框架,Ba^{2+}作为阳离子填隙其中。基于密度泛函理论计算了该化合物的能带结构和态密度,结果表明该化合物是窄带隙半导体(E_g=0.4 eV)。另外,DSC 和变温 XRD 结果表明高温下 α-$BaZn_2P_2$ 分解为 Ba_4P_5,ZnP_4 等二元相。

关键词:Zintl 相化合物;磷族化合物;晶体结构;电子结构

中图分类号:O614.23+3;O614.24+1 **文献标识码**:A **文章编号**:1001-4861(2018)02-0277-06

DOI:10.11862/CJIC.2018.056

Synthesis, Structure, and Properties of Zintl Phase Compound α-$BaZn_2P_2$

BAI Ming-Cheng[1,2] PAN Ming-Yan[2] WANG Lin*[,1] QI Hong-Ji[2] WANG Hu[2]

([1]*School of Materials Science and Engineering, Shanghai University, Shanghai* 200444, *China*)

([2]*Key Laboratory of Materials for High Power Laser, Shanghai Institute of Optics and Fine Mechanics, Chinese Academy of Sciences, Shanghai* 201800, *China*)

Abstract: A Zintl phase compound α-$BaZn_2P_2$, was synthesized through the high-temperature Sn-flux reaction. Single-crystal X-ray diffraction was used to accurately determine its structure, which is similar to α-$BaCu_2S_2$-type structure (*Pnma*). The cell parameters of α-$BaZn_2P_2$ are a=0.976 78(5) nm, b=0.413 34(2) nm, c=1.060 55(5) nm. Unlike high-temperature-phase β-$BaZn_2P_2$, which has a layer structure, low-temperature-phase α-$BaZn_2P_2$ has a three-dimensional network structure, where ZnP_4 tetrahedra form an anion frame by sharing sides or vertices, with Ba^{2+} cations residing within. The band structure and state density of the compound were calculated using density functional theory. The results indicate that the compound is a narrow-bandgap semiconductor (E_g=0.4 eV). In addition, differential scanning calorimetry and temperature-dependent XRD results show that α-$BaZn_2P_2$ decomposes into binary phases like Ba_4P_5 and ZnP_4 at high temperatures. CCDC: 433850.

Keywords: Zintl phase compound; phosphorus compounds; crystal structure; electronic structure

0 Introduction

Zintl phase compounds are special polar intermetallics comprising metals with very different electronegativities, and the electropositive elements can usually be assumed to completely transfer their valence electrons to the electronegative ones; thus, each constituent atom obeys the 8-N octet rule and a

收稿日期:2017-09-08。收修改稿日期:2017-12-22。

国家自然科学基金(No.11304193,11375112)资助项目。

*通信联系人。E-mail:wanglinn@shu.edu.cn

closed-shell configuration is achieved. Such an electron-precise nature has been observed frequently in Zintl phases, and plays a critical role in governing the formation of the structures of these compounds[1-4]. Because of their complex crystal structures, Zintl phase compounds exhibit specific physical and chemical properties. For example, $Yb_{14}MnSb_{11}$[5-6], which has a high molecular mass of 3 783.088 and very low thermal conductivity, has a figure of merit (zT) of 1.0 at 1 200 K. $BaFe_2As_2$, another Zintl compound, with a tetragonal $ThCr_2Si_2$-type structure and space group *I*4/*mmm*, has been reported to show great superconductivity. It exhibits a structural and magnetic phase transition at 140 K, at which a spin-density-wave anomaly has been observed, and the superconducting transition temperature can be increased to 38 K by doping with $K((Ba_{1-x}K_x)Fe_2As_2$, x=0.4)[7-9]. Many other Zintl phase compounds exhibit excellent thermoelectric performances, magnetic properties, and superconductivities.

The formula RM_2X_2 (R=rare or alkaline earth metal, M=metal, and X=group ⅢA ~ ⅥA element) represents a very large family of compounds with more than five crystal types (*I*4/*mmm*, $P\bar{3}m1$, *Pnma*, and *Cmcm*)[10]. RM_2X_2 compounds crystallize mainly into the structure of $ThCr_2Si_2$[7], with the tetragonal space group *I*4/*mmm*, and contain practically identical layers of edge-sharing MX_4 tetrahedra separated by R atom layers. The second-most common crystal structure of RM_2X_2 compounds is the $CaAl_2Si_2$-type structure[11], with the space group $P\bar{3}m1$. The trigonal structure for these RM_2X_2 compounds can be viewed as polyanionic M_2X_2 layers stacked along the *c*-axis and separated by layers of R cations[12]. The least common crystal structure among RM_2X_2 compounds is the α-$BaCu_2S_2$-type structure[13-14], with an orthogonal phase featuring the *Pnma* space group, in which MX_4 tetrahedra form a three-dimensional (3D) network frame with large cavities where R cations are located.

The different structure types are closely connected, and phase transitions may occur between them. For example, $BaAl_2Ge_2$[15] and $BaCu_2S_2$ undergo a reversible phase change process, where the α (low-temperature phase; space group *Pnma*) phase changes to the β (high-temperature phase; space group *I*4/*mmm*) phase when the temperature rises, and the reverse occurs when the temperature is lowered. For $BaZn_2P_2$, the high-temperature phase (group *I*4/*mmm*) was reported in 1978[16], but the low-temperature phase has not been reported yet. In this study, α-$BaZn_2P_2$ was obtained via the high-temperature Sn-flux reaction. The synthesis, crystal structure, and electronic band structure of α-$BaZn_2P_2$ are presented and discussed in this paper, and the results of differential scanning calorimetry (DSC) and temperature-dependent X-ray diffraction (XRD) show that thermal decomposition occurs during the heating process.

1 Experimental

1.1 Synthesis

All manipulations were performed either in an argon-filled glovebox or under vacuum. The starting materials P (99.999%), Zn (99.99%), Ba (99+%), and Sn (99.9%) were obtained from Alfa and used as received. The elements, Ba, Zn, P, and Sn, were arranged in an alumina crucible in a molar ratio of 2∶1∶3∶20. The reactions were sealed in quartz ampoules under vacuum, and the ampoules were placed in a high-temperature programmable furnace. The reactions were heated to 300 ℃ over 5 h, and held at that temperature for an additional 5 h. Afterwards, the sealed mixtures were heated to 950 ℃ and held at that temperature for 20 h, and then slowly cooled to 400 ℃ at a rate of −5 ℃·h^{-1}. Then, they were centrifuged at 2 500 r·min^{-1} for 5 min to separate the products from the Sn flux. The main products were silver block crystals of $Ba_3Sn_2P_4$ and needle crystals of α-$BaZn_2P_2$. The α-$BaZn_2P_2$ crystals were stable in air, water, and alcohol, and reacted slowly with dilute acid.

1.2 X-ray powder diffraction

Powder XRD patterns were obtained at room temperature using an Ultima Ⅳ X-ray powder diffractometer using Cu $K\alpha$ radiation (λ=0.154 18 nm). The operating voltage and current were 40 kV and 40 mA, respectively. The data were recorded in 2θ mode with a step size of 0.02° and a counting time of 10 s,

and the scanning range was from 20° to 80°. The results were used for the phase purity analysis only.

Temperature-dependent XRD was conducted using an Empyrean with a temperature platform in order to analyze the changes in α-$BaZn_2P_2$ during the heating process from 30 to 920 ℃. A powdered sample was placed on the platform and heated at 10 ℃·min^{-1} from room temperature. Measurements were taken at 30, 200, 400, 600, 800, 850, 870, 900 and 920 ℃ and the results were compared with DSC.

1.3 Single-crystal X-ray diffraction

Single crystal of the title compound were selected and cut in Patatone-N oil to suitable size (0.3 mm×0.06 mm×0.06 mm) and then mounted on glass fiber for data collection, which was performed on a Bruker SMART APEX-Ⅱ CCD area detector with graphite-monochromated Mo $K\alpha$ radiation (λ=0.071 073 nm) at 296 K using ω scan. Data reduction and integration, along with global unit cell refinements, were performed by the INTEGRATE program incorporated in the APEX2 software. Semi-empirical absorption corrections were applied using the SCALE program for the area detector. The structures were solved using direct methods and refined using full matrix least-squares methods on F^2 using SHELX-2014[17]. All structures were refined to converge with anisotropic displacement parameters.

CCDC: 433850.

1.4 Elemental analysis

Several single crystals of the title compound were selected and energy dispersive X-ray spectroscopy (EDS) measurements were performed using a Zeiss Auriga scanning electron microscope with an energy dispersive spectrometer to determine the elemental composition. The spectra obtained from visibly clean surfaces provided results identical to those of the crystallographic data. The compositions were homogeneous within one crystal, and, within standard uncertainty, identical to those of crystals selected at random from different reactions (Supporting Information).

1.5 Thermogravimetry (TG)/DSC

A Netzsch Thermal Analysis STA 449 F3 Jupiter® was used to evaluate the thermal properties of α-$BaZn_2P_2$ between 50 and 950 ℃. After a baseline was established, 166.598 6 mg of prepared powdered sample was placed in an alumina crucible and heated under argon at 10 K·min^{-1}.

1.6 Calculation of electronic and energy band structures

The calculations were based on density functional theory (DFT) and used first-principles approaches. Similar calculation results for $BaZn_2As_2$ were reported by Shein et al in 2014[18]. The Vienna *ab initio* simulation package using the projector augmented wave method was used to calculate the equilibrium structural parameters and elastic properties of the polymorphs[19-20]. The exchange correlation potentials were calculated using the Perdew-Burke-Ernzerhof generalized gradient approximation (PBE-GGA)[21]. A kinetic energy cutoff of 500 eV and k-mesh of 5×10×5 for an orthorhombic structure were used. The geometry optimization was performed with a force cutoff of 10 meV·nm^{-1}.

2 Results and discussion

2.1 Structure description

The α-$BaZn_2P_2$ single crystals were prepared via a Sn-flux reaction. The EDS results were consistent with the stoichiometry as written. Single-crystal X-ray diffraction confirm that $BaZn_2P_2$ crystallizes with the α-$BaCu_2S_2$-type structure (space group *Pnma*). Crystallographic data and structural refinements are summarized in Table 1. The cell parameters are a=0.976 78 (5) nm, b=0.413 34 (2) nm, c=1.060 55(5) nm. Selected atomic positional and displacement parameters are shown in Table S1, and the most important interatomic distances and angles are presented in Table S2.

The crystal structures of α- and β-$BaZn_2P_2$ are shown in Fig.1; the Ba atoms are orange, Zn atoms are yellow, and P atoms are green. As shown in Fig.1 (a), α-$BaZn_2P_2$ features a 3D network of Zn and P atoms that form large cavities in which Ba atoms reside. Ba is in seven-fold coordination with respect to Zn, with Ba-Zn distances ranging from 0.326 17(7) to 0.364 30(6) nm (distances here and later in the article were obtained from X-ray data at 296 K). Seven P

Table 1 Crystal data and structure refinement for α-$BaZn_2P_2$

Formula	$BaZn_2P_2$	V / nm^3	0.428 19(4)
Formula weight	330.2	Z	4
Crystal system	Orthorhombic	D_c / (g·cm^{-3})	5.119
Space group	*Pnma*	GOF	1.04
a / nm	0.976 78(5)	Final R indices [$I>2\sigma(I)$][a]	R_1=0.025 8, wR_2=0.063 9
b / nm	0.413 34(2)	Final R indices (all data)[a]	R_1=0.025 8, wR_2=0.064 0
c / nm	1.060 55(5)		

[a] $R_1=[\sum||F_o|-|F_c||]/\sum|F_o|$, $wR_2=[\sum w(|F_o^2|-|F_c^2|)^2]/\sum w(|F_o|^2)^2]^{1/2}$

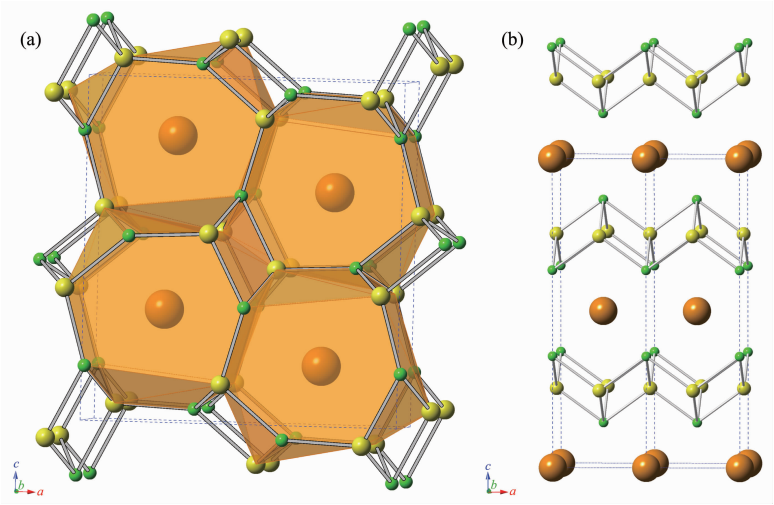

Ba, Zn, and P atoms are shown in orange, yellow, and green, respectively

Fig.1 (a) Polyhedral and ball-and-stick models of the crystal structure of α-$BaZn_2P_2$; (b) Ball-and-stick model of β-$BaZn_2P_2$

atoms surround each Ba, and the Ba-P distances range from 0.319 66(14) to 0.350 26(12) nm. The Zn1 and Zn2 atoms both have tetrahedral coordination with P atoms, with Zn-P distances ranging from 0.243 26(8) to 0.255 04(15) nm. The polyhedral view with ZnP_4 tetrahedra is shown in Fig.S1. Fig.S1(a) shows that the ZnP_4 tetrahedra form the anion frame by sharing sides or vertices and that Ba^{2+} cations are located in the large cavities. Fig.S1(b,c) show the chains in the b-axis formed by sharing sides of Zn1- and Zn2-centered ZnP_4 tetrahedra . Fig.S1(d) shows the cavity where Ba atoms are located; the cavities were formed through the sharing of the vertices (P atoms) of the ZnP_4 tetrahedra. The bond angles of ZnP_4 tetrahedra are presented in Table S2, and are 94°~117° for Zn1, 106°~115° for Zn2, 84°~143° for P1, and 73°~138° for P2.

For comparison, Fig.1(b) shows the ball-and-stick model of β-$BaZn_2P_2$, which crystallizes in a tetragonal phase, with the $ThCr_2Si_2$-type structure and the space group *I*4/*mmm*. The high-temperature β phase of $BaZn_2P_2$ contains layers of edge-sharing ZnP_4 tetrahedra separated by Ba atom layers (Fig.S1(e,f)).

2.2 XRD

XRD was conducted for α-$BaZn_2P_2$, and the results are shown in Fig.2(a). For comparison, the calculated XRD patterns of α-$BaZn_2P_2$ (*Pnma*) and β-$BaZn_2P_2$ (*I*4/*mmm*) are shown in Fig.2(b) and 2(c), respectively. Fig. 2 shows that the collected samples are α-$BaZn_2P_2$ (*Pnma*); the small peaks indicated with an asterisk (*) in the collected data curve are Sn peaks. The α-$BaZn_2P_2$ peak (2θ =32.23°) in the collected data spectrum is very intense because it partially overlaps with a Sn peak (2θ=32.04°).

Fig.3 shows the temperature-dependent XRD results. As the temperature increased to 920 ℃, α-$BaZn_2P_2$ was basically retained, while the peak positions were shifted to the left and the small peaks of α-$BaZn_2P_2$ shrank and gradually disappeared. During the

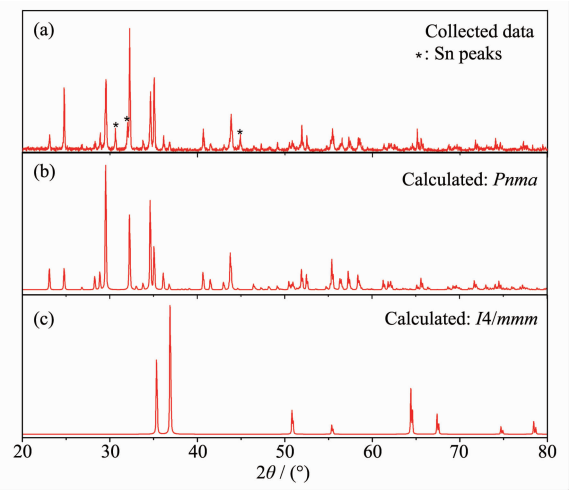

Fig.2　XRD pattern of α-$BaZn_2P_2$ single crystals ground into a powder (a), calculated XRD patterns of α-$BaZn_2P_2$ with space group *Pnma* (b) and β-$BaZn_2P_2$ with space group *I*4/*mmm* (c)

experiment, the general structure of α-$BaZn_2P_2$ was retained even at 920 ℃. However, with the increase in temperature during the heating process, the atomic vibration of α-$BaZn_2P_2$ increased, the interplanar spacing became larger, and the degree of disorder increased. At the same time, the main peak ($2\theta \approx 29°$) of α-$BaZn_2P_2$ indicate cleavage with increasing temperature, which was the result of the exacerbation of atomic vibration.

In addition, the peaks changed during the heating process (Fig.3). At 30 ℃, the main species is α-$BaZn_2P_2$ with a bit of Sn (small peaks indicated with a triangle △), and the Sn peaks disappeared when the temperature reached 400 ℃. When the temperature reached 800 ℃, some new peaks of Ba_4P_5 appeared,

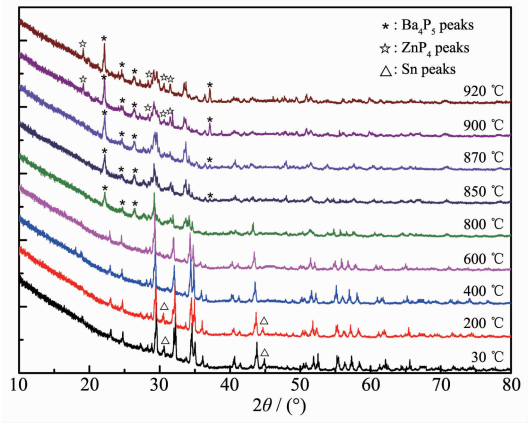

Fig.3　Temperature-dependent XRD patterns of α-$BaZn_2P_2$ from 30 to 920 ℃

which were indicated with an asterisk (*). When the temperature reached 900 ℃, new peaks of ZnP_4 appeared, which were indicated with a white star (☆), and there may be some other new binary phases. Therefore, α-$BaZn_2P_2$ can decompose during the heating process. This is consistent with the results of DSC.

2.3　Thermal stability analysis

Differential thermal analysis (DTA) and TG experiments were performed over the 50 ~950 ℃ temperature range with the sample under the protection of an Ar atmosphere, and the results are presented in Fig.4. For α-$BaZn_2P_2$, no significant mass loss was observed in the TG curve over the entire measured temperature range, and the endothermic peak appearing at around 230 ℃ in the DSC curve should be attributed to the melting of remaining Sn from the flux. The endothermic peaks appearing at around 860 ℃ in the DSC curve indicate the decomposition of α-$BaZn_2P_2$, which results in binary phases such as Ba_4P_5 and ZnP_4, as confirmed by XRD patterns.

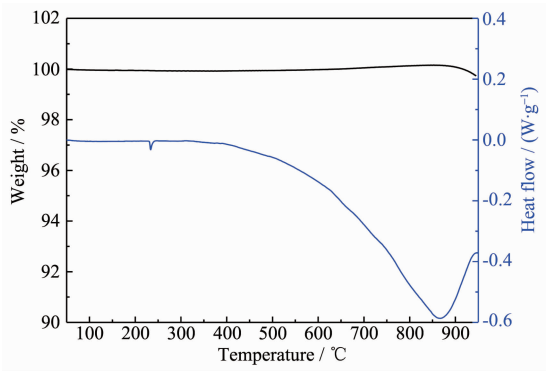

Fig.4　TG (black) and DSC (blue) curves for α-$BaZn_2P_2$

2.4　Electronic and energy band structure calculations

To understand better the properties of the new Zintl phase, electronic structure calculations were performed for α-$BaZn_2P_2$. The results are presented in Fig.5. α-$BaZn_2P_2$ has a small bandgap of approximately 0.4 eV, typical for a narrow-bandgap semiconductor. In Fig.5(a), the electrons in the 4*d* orbitals of Ba atoms are still in the conduction band, while those in the *s* and *p* orbitals are all transferred to Zn or P atoms. In the ZnP_4 tetrahedron structures in α-$BaZn_2P_2$, Zn^{2+} provides four unoccupied orbitals with the lowest

energy and forms coordination bonds (Zn-P bonds) with P. So Fig.5(a) shows the orbital hybridization, which should be sp^3 hybridization. The energy band structures are presented in Fig.5(b), and direct transitions were found in this semiconducting material.

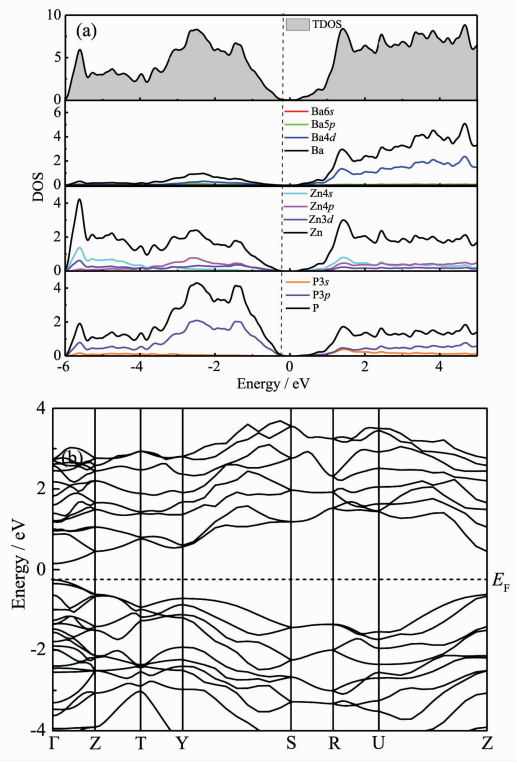

Fermi energy was chosen for energy reference in (a)

Fig.5 (a) Calculated total density of states (TDOS) and partial density of states (PDOS) for various constituent atoms in α-$BaZn_2P_2$; (b) Energy band structures of α-$BaZn_2P_2$

3 Conclusions

A new Zintl phase compound, α-$BaZn_2P_2$, with the space group *Pnma* was synthesized through metal-flux reactions. The structure was accurately determined using single-crystal XRD techniques. α-$BaZn_2P_2$ has a three-dimensional network structure, where ZnP_4 tetrahedra form an anion frame by sharing sides or vertices, with Ba^{2+} cations residing within. There was no phase transition, but decomposition occurred during the heating process. The electronic and energy band structures were calculated in order to understand clearly the properties of α-$BaZn_2P_2$. The energy gap was approximately 0.4 eV, which indicates that α-$BaZn_2P_2$ is a narrow-bandgap semiconductor.

Supporting information is available at http://www.wjhxxb.cn

References:

[1] Miller G J, Schmidt M W, Wang F, et al. *Struct. Bond.*, **2011**,**139**:1-57

[2] Wang F, Miller G J. *Inorg. Chem.*, **2011**,**50**:7625-7636

[3] Bojin M D, Hoffmann R. *Helv. Chim. Acta*, **2003**,**86**:1653-1682

[4] Pan M Y, Xia S Q, Liu X, et al. *Eur. J. Inorg. Chem.*, **2015**, **46**(33):2724-2731

[5] Brown S R, Kauzlarich S M, Gascoin F, et al. *Chem. Mater.*, **2006**,**18**(7):1873-1877

[6] ZHAO Li-Dong(赵立冬). *Journal of Xihua University*: *Natural Science Edition*(西华大学学报:自然科学版), **2015**(1):1-13

[7] Ban Z, Sikirica M. *Acta Crystallogr.*, **1965**,**18**:594-599

[8] Rotter M, Pangerl M, Tegel M, et al. *Angew. Chem. Int. Ed.*, **2008**,**47**(41):7949-7952

[9] Rotter M, Tegel M, Johrendt D, et al. *Phys. Rev. B*, **2008**,**78** (2):1436-1446

[10]Condron C L, Hope H, Piccoli P M, et al. *Inorg. Chem.*, **2007**,**46**(11):4523-4529

[11]Gladyshevskii E I, Kripyakevich P I, Bodak O I. *Ukr. Fiz. Zh.*, **1967**,**12**:447-452

[12]Sun J, Singh D J. *J. Mater. Chem. A*, **2017**,**5**(18):8499-8509

[13]Iglesia J E, Pachali K E, Steinfink H. *J. Solid State Chem.*, **1974**,**9**(1):6-14

[14]Huster J, Bronger W. *Z. Anorg. Allg. Chem.*, **1999**,**625**:2033-2040

[15]Leoni S, Carrillo-Cabrera W, Schnelle W, et al. *Solid State Sci.*, **2003**,**5**(1):139-148

[16]Klüfers P, Mewis A. *Z. Naturforsch., B*: *Chem. Sci.*, **1978**,**33** (2):151-155

[17]Sheldrick G M. *SHELX*-2014, *Program for the Solution and the Refinement of Crystal Structures*, University of Göttingen, Germany, **2014**.

[18]Shein I R, Ivanovskii A L. *J. Alloys Compd.*, **2014**,**583**:100-105

[19]Kresse G, Joubert D. *Phys. Rev. B*, **1999**,**59**(3):1758-1775

[20]Kresse G, Furthmuller J. *Phys. Rev. B*, **1996**,**54**(16):11169-11186

[21]Perdew J P, Burke S, Ernzerhof M. *Phys. Rev. Lett.*, **1996**, **77**(18):3865-3868